Special Issue: DTD 2006 in JAPAN
Original Article
J. Jpn. Soc. Microgravity Appl. Vol. 24 No. 3 2007 (225-230)

Effect of Ambient Gas on Flame Spread over a Solid Material in Microgravity

Shuhei TAKAHASHI[1], Subrata BHATTACHARJEE[2],
Tadayoshi IHARA[1], and Kazunori WAKAI[1]

[1] Gifu University, Gifu, Japan, shuhei@gifu-u.ac.jp
[2] San Diego State University, San Diego, USA, subrata@thermo.sdsu.edu

Abstract

The flame spread rate over a PMMA film was measured with varying ambient balance gas, N_2, CO_2, He and Ar, in normal gravity and microgravity. A scale analysis was also conducted to discuss how ambient flow velocity, V_g, and gas properties affect the flame behavior. With decreasing the V_g, the flame behavior moves to the microgravity-regime from the thermal-regime. However, the V_g at which the regime switches is different according to the ambient gas properties. In Ar and CO_2 balances, the flame is robust even with very low V_g because of their small preheat-zone length, L_g, high flame temperature, T_f, or high absorption coefficiency, α_{abs}. On the other hand, in He balance, the L_g is so large that the range of V_g where the thermal-regime is held is very narrow, which results in weak flame both in normal gravity and microgravity. This result implies that not only the V_g but also the gas properties must be taken into account to discuss the flame spread in microgravity. The dimensionless heat loss number proposed by the present scale analysis gives good help to estimate the "critical flow velocity" below which the flame cannot spread.

1. Introduction

Flame spread over a solid material under microgravity condition is characterized by the low ambient flow around the flame. In such condition, characteristic length of the flame, such as the preheat zone lengths, the flame height and so on, increase and the behavior of the flame changes compared with that under normal gravity. For example, it was found in our previous study[1)] that the preheat zone length of downward flame spread in normal gravity was about 3mm, whereas it increased about 9 times, to 26mm in a quiescent microgravity condition.

We have investigated the influence of flame size on the spread rate over a solid material by scale analysis[2-6)]. The results show that the enlarged characteristic lengths of the flame cause large heat loss to the surroundings and suppress the flame spread especially through radiation. Similar results have been reported by other researchers[7,8)], and numerical simulations[7,9)] also suggest that radiative losses are responsible for the quenching branch. Therefore, the fire hazard in microgravity tends to go to "safe side" than in normal gravity. In other words, the microgravity condition has suppression effect and the flame in microgravity is weaker than that in normal gravity. Then, where is the boundary between the microgravity-regime and the thermal-regime? Does only the ambient flow velocity define it?

In this study, we measured the flame spread rate over a thin PMMA film with varying the ambient flow velocity and the ambient gas composition. We used N_2, CO_2, He, and Ar as a diluent gas, and investigated how the suppression effect appeared with decrease of the ambient flow velocity, and discussed the "critical flow velocity."

2. Experimental Setup

The apparatus was a closed-type wind tunnel, which is 37cm in length, 12cm in width, and 24cm in height (**Fig. 1**). This wind tunnel had a small fan driven by a brushless DC motor to create slow ambient flow, V_g, in a range of 0~16cm/s. The PMMA sample (ACRYPLEN™ by Mitsubishi Rayon Co., Ltd.) was attached at the sample holder, and the size of the sample used was 8cm(L) x 1cm(W). The sample was ignited with an electrically heated Ni-Cr wire at upstream end for the concurrent flow configuration, or at downstream end for the opposed flow configuration. After the ignition, the wire was removed by a spring. The ignition of the sample was preformed 2.0s before the drop. The thickness of the sample was 125μm (=1/8mm).

We used N_2, CO_2, He, and Ar as the balance gas. The properties of each gas are shown in Table 1. The oxygen level was varied at 21%, 30% and 50%. The flame spread was recorded with a CCD camera. In order to define the preheat zone length, the temperature field around the flame was measured with Michelson interferometer system. (see **Fig. 2**) The microgravity condition was obtained with the MGLAB's 4.5s drop tower in Toki, Japan. The g-jitter is less than 10^{-5} g.

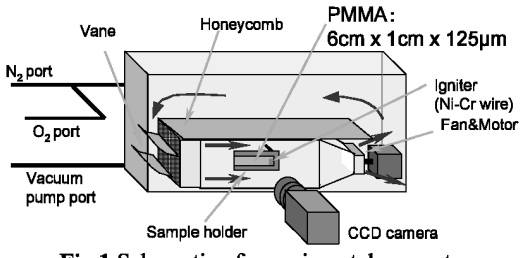

Fig.1 Schematic of experimental apparatus

Table 1 Properties of diluent gas[10),11)]

	Cp [J/mol K]	λ_g [W/m K]	α_g [mm^2/s]	Absorption band [μm]
N_2	29.06	0.0249	21.1	-
CO_2	37.2	0.0164	10.9	4.4
He	20.78	0.158	186.6	-
Ar	20.78	0.0178	21.1	-

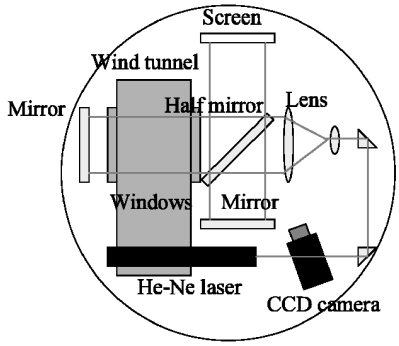

Fig.2 Layout of the interferometer system

3. Scale Analysis

Figure 3 shows the schematic of the flame used for the scale analysis. Since ACRYPLEN™ has similar thermodynamic properties of PMMA, we use typical PMMA's properties in the scale analysis; the density, the specific heat capacity and the thermal conductivity are 1190kg/m^3, 1.465kJ/kgK and 0.188W/mK, respectively. In the thermal-regime, the dominant path of the heat flow is heat conduction from gas phase to the solid phase. Therefore, the spread rate, V_f, is derived from Eq. 1, and expressed as Eq. 2.

$$V_{f,th}\rho_s c_s L_{sy} W(T_v - T_\infty) \sim \lambda_g \frac{(T_f - T_v)}{L_{gy}} L_{gx} W \qquad \text{Eq. 1}$$

$$V_{f,th} \sim \frac{\lambda_g}{\rho_s c_s \tau} F \quad \text{where} \quad F \equiv \frac{T_f - T_v}{T_v - T_\infty} \qquad \text{Eq. 2}$$

The preheat zone lengths are described as Eq. 3, and it is found that they are proportional to the inverse of the ambient flow velocity, V_r^{-1}.

$$L_{gx} = L_{gy} = \alpha_g / V_r \qquad \text{Eq. 3}$$

If we consider the loss due to radiation and side effect (3D effect), Eq. 1 is rewritten as Eq. 4 and it can be non-dimensionalize as Eq. 5.

$$V_f \rho_s c_s L_{sy} W(T_v - T_\infty) + Q_{loss} \sim \lambda_g \frac{(T_f - T_v)}{L_{gy}} L_{gx} W \qquad \text{Eq. 4}$$

$$\eta + R_{loss} = 1 \quad \text{where} \quad \eta \equiv V_f / V_{f,th} \qquad \text{Eq. 5}$$

For R_{loss}, the followings show the dimensionless heat loss from the solid phase to the environment by radiation, and the loss from gas phase to the spanwise direction by conduction, respectively.

$$R_{loss} = R_{rad} + R_{side} \qquad \text{Eq. 6}$$

where

$$R_{rad} = \frac{\varepsilon(1-\alpha_{abs})\sigma\left(T_v^4 - T_\infty^4\right)}{\rho_g c_g V_r \left(T_f - T_v\right)} \propto (1-\alpha_{abs})\frac{1}{V_r} \qquad \text{Eq. 7}$$

$$R_{side} = 4\left(\frac{L_g}{W}\right)^2 \frac{T_f - T_\infty}{T_f - T_v} \propto \left(\frac{\alpha_g}{V_r W}\right)^2 \qquad \text{Eq. 8}$$

It is found that these losses are function of the preheat zone length, L_g, thermal diffusivity, α_g and ambient flow velocity, V_r. In normal gravity, the L_g is so small and V_r is so large that we can neglect the loss effects. However, when the V_r is close to zero under microgravity condition, the flame size increases and these heat loss factors become significant.

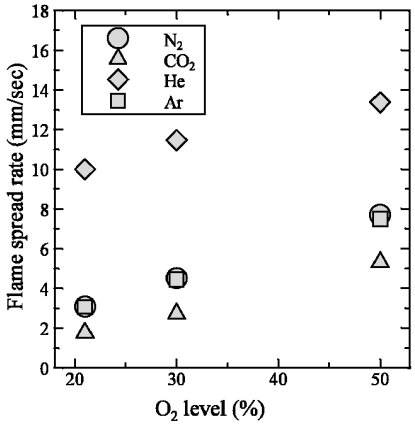

Fig.4 Predicted downward spread rate

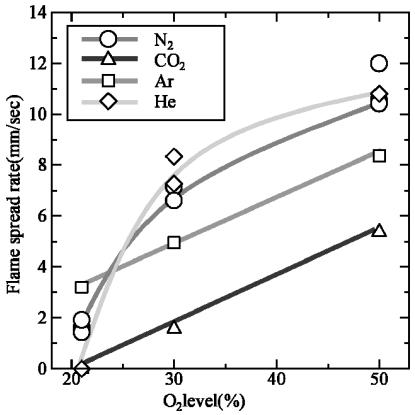

Fig.5 Experimental downward spread rate

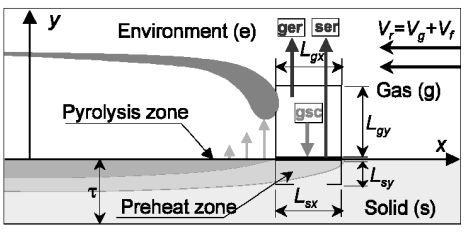

Fig.3 Schematic of flame spread

4. Results and Discussions

4.1 Downward spread in normal gravity

Figures 4 and **5** show the analytical prediction and experimental downward flame spread rate in thermal-regime under each balance gas condition. No additional forced flow is present; that is the ambient flow is buoyant flow only. The analytical results are obtained by EST equations[2] based on Eq. 2.

$$V_{f,thin,EST} = \frac{c_{hd}\pi}{4}\left(\frac{\lambda_g}{\rho_s c_s \tau}\right)\left(\frac{T_{f,ad,deRis} - T_v}{T_v - T_\infty}\right) \quad \text{Eq. 9}$$

where $C_{hd} = 1 + 1.324 l_{hd} - 0.684 l_{hd}^{\ 2}$

$$l_{hd} = 1.365\exp(-7.463\frac{\beta_1}{\ln(1+B)})$$

$$\beta_1 = \frac{y_{O,\infty}}{s} = 0.278,\ B = 7.24$$

The predicted spread rate is He>N2~Ar>CO_2. This result is clearly caused by the effect of He's large heat conductivity, λ_g, and large F due to small heat capacity, and CO_2's large heat capacity that results in small F. The experimental results agreed with the prediction at high O_2 level condition, such as 30% and 50%. This implies that at high O_2 level, the flame behaviors are explained with the theory of thermal-regime and the loss effects in Eqs. 7 and 8 are not significant.

At low O_2 level, 21%, however, the tendency changed and the spread rates was Ar>N_2>He~CO_2. No flame spread was observed in He and CO_2 balance conditions. In He balance condition, the flame behavior recorded with CCD camera showed that the blow-off occurred whereas extinction occurred in CO_2 balance.

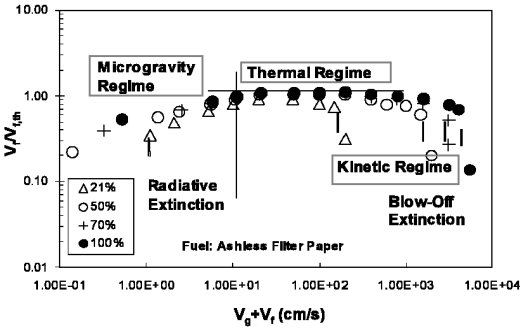

Fig.6 Computational spread rate at different oxygen level

This result can be interpreted as follows. At low O_2 level, such as 21%, the chemical reaction is not so fast and flame behavior may shift to kinetic-regime from the thermal-regime, that results in Damkohler number extinction[12,13]. **Figure 6** shows the numerical result of spread rate over a ashless paper in our previous research. This plot shows that the boundary between the thermal-regime and the kinetic-regime changes with the O_2 level. The boundary is determined by the Damkohler number, Da.

$$Da \equiv t_{res}/t_{chem} = (L_g/V_r)/(\rho/\dot{\omega}) \propto \exp(-E/RT_f)/V_r^2 \quad \text{Eq. 10}$$

Therefore the kinetic-regime limit is influenced by the flame temperature and the ambient flow velocity.

In Ar balance condition, the flame temperature is high due to its low heat capacity that results in robust flame even at low O_2 level. On the other hand, in CO_2 balance, the flame temperature is low and it causes extinction. In He balance, the flame temperature is not so low, but the ambient buoyant flow is anticipated higher than the other balance gas condition because the ambient buoyant flow velocity is roughly estimated by the following expression[3].

$$V_g \sim \sqrt[3]{g\alpha_g \frac{T_v - T_\infty}{T_\infty}} \quad \text{Eq. 11}$$

It is found the He's large thermal diffusivity induces relatively large buoyant flow, and it is estimated 1.5 times larger (~60cm/s) than those in the other conditions (~40cm/s). This means that the flame in He balance may be already in the kinetic-regime with the buoyant flow. Thus, the flames in N_2 and Ar balance conditions are still remains in the thermal-regime, but the flames in He and CO_2

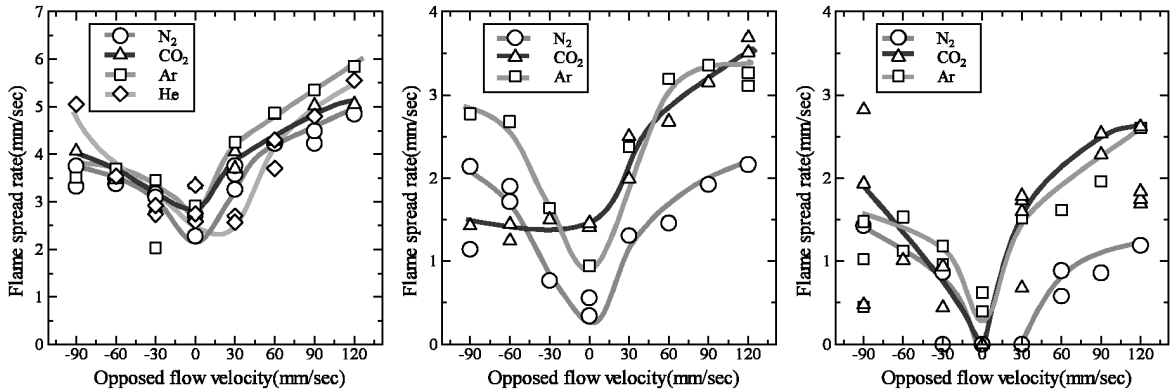

a) O_2 level: 50% b) O_2 level: 30% c) O_2 level: 21%

Fig.7 Flame spread rate in microgravity with varying ambient flow velocity

balance conditions are moved to the kinetic-regime at 21% O_2 level. In all conditions, the flame spread in CO_2 balance was lowest, and this proved CO_2's high performance of extinguishant under normal gravity.

4.2 Flame spread in microgravity

Figure 7 shows the spread rate in microgravity with varying ambient flow velocity. The trend of the flame spread was quite different from that in normal gravity. Only at 50% O_2 level, flame spread was observed for all balance gas conditions. Near a quiescent condition, the spread rate was CO_2>Ar>N_2~He; the flame in CO_2 balance was robustest and that in He balance was weakest. If there exists relatively large ambient flow (~12cm/s), the trend changed; Ar>He>CO_2>N_2. When the O_2 level was low (30% and 21%), the He balance condition did not allow flame spread at all ambient velocities in Fig. 7. The robust flame was also observed in CO_2 balance near a quiescent condition at low O_2 level.

Figure 8 shows the interferometer images in a quiescent condition and with V_g=16cm/s. The preheat zone length, L_g, is superimposed. The L_g is expressed as Eq. 3 and it increases if the V_g goes to zero. The result shows larger L_g in a quiescent condition than in V_g=16cm/s. Additionally, the L_g is also affected by the thermal diffusivity of the ambient gas, α_g. Therefore, the L_g is quite different among four balance gas conditions. It is emphasized that the flame in He balance has quite large L_g whereas that in CO_2 balance has small one. The L_g in He balance at V_g=16cm/s is almost same as that in N_2 balance in a quiescent condition. The large L_g in He balance and the absorption characteristics of CO_2 result in the significant shift of the boundary between thermal-regime and the microgravity-regime.

The robust flame near a quiescent condition in CO_2 balance and the weak flame in He balance deserve to mention. Additionally, the Ar balance flame was robust through all conditions conducted in this experiment. These features are explained as shown in Fig. 9. **Figure 9** shows the calculated dimensionless heat losses according to Eqs. 7 and 8. The extinction limit of the flame spread in the microgravity-regime can be estimated with Eq. 5. Therefore, if the R_{loss}(~R_{rad}+R_{side}) is close to unity, extinction occurs. For He balance condition, the diffusivity is so large that it is expected that the loss due to side effect becomes significant with relatively high ambient flow as well as radiative loss. This consistent with the large L_g with V_g=16cm/s in He balance in Fig. 8. Therefore, for the flame in He balance, microgravity-regime comes at relatively large V_g. This feature overcomes the enhancement effect of large λ_g and flame spread is suppressed as a result.

On the other hand, for CO_2 balance, the size of the L_g is smallest among the four conditions. Additionally, CO_2 has a strong absorption band near 4.4μm that causes re-absorption effect[14] and decreases the radiative loss. Thus, for the flame in CO_2 balance, the radiative loss and the side loss are small, and the thermal-regime lasts even at very low V_g. This results in robust flame in spite of low T_f due to large Cp.

For Ar balance condition, the preheat zone length, the heat conductivity and the diffusivity are almost same as those in N_2 balance, but the heat capacity is smaller. The small Cp results in high flame temperature, T_f, and this sustains the thermal-regime at very low V_g compared with N_2

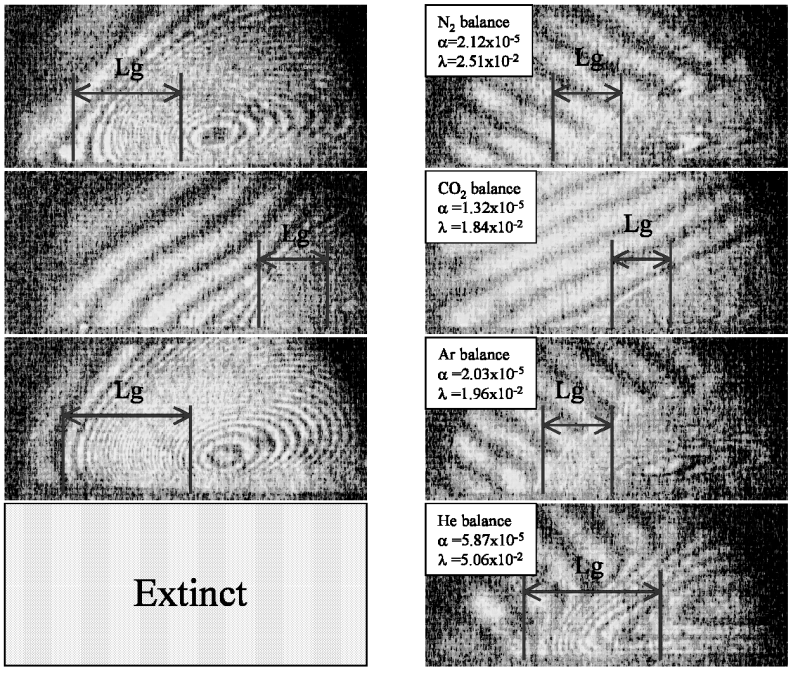

a) V_g=0cm/s b) V_g=16cm/s

Fig.8 Interferometer images (O_2 level: 30%)

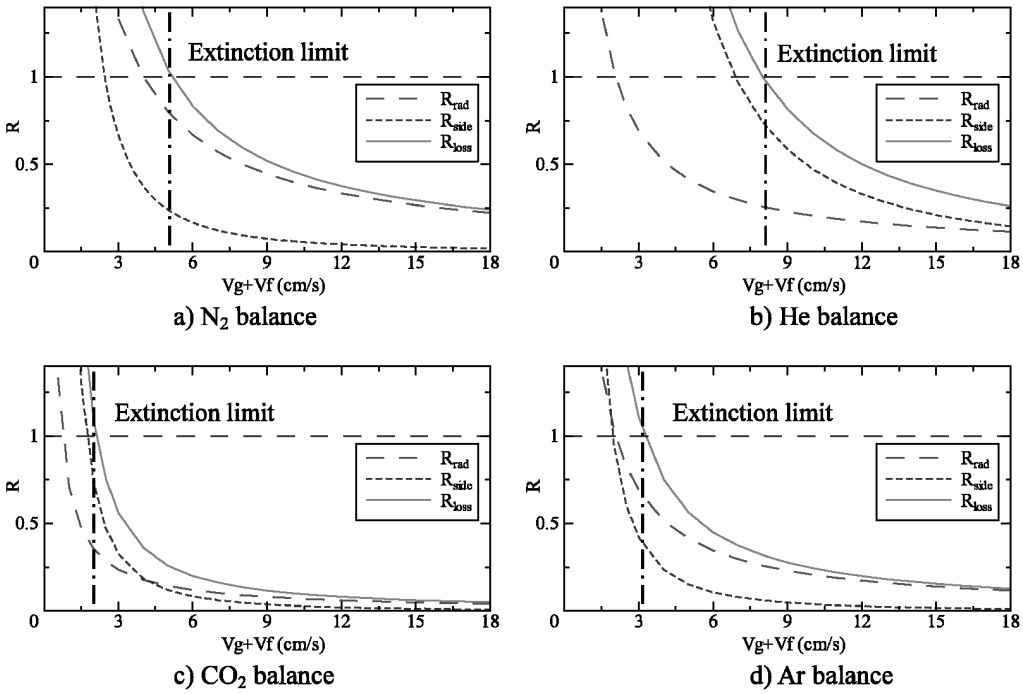

Fig.9 Dimensionless heat loss vs. opposed flow velocity (O_2 level: 21%)
Long dash: R_{rad}, Short dash: R_{side}, and Solid: R_{loss}

balance condition. The calculation in Fig. 9 is very simple and rather qualitative, but it can well explain the experimental result in Fig. 7.

5. Conclusions

The flame spread rate over a PMMA film was measured with varying ambient balance gas, N_2, CO_2, He and Ar, in normal gravity and microgravity. The result shows that the ambient flow velocity at which the regime switches to the microgravity-regime is quite different among these four balance gas conditions. This difference is caused by their thermodynamics properties of the ambient gas and their absorption characteristics. The impacts of the properties on the flame spread are as follows;

Conductivity:

Large conductivity can enhances the spread rate in normal gravity, but it also may suppress the spread due to the large heat loss to the side that results from large flame size in microgravity.

Heat capacity:

Large heat capacity reduces the flame temperature and suppresses the flame spread both in normal gravity and microgravity. However, the gas with large heat capacity has large degree of freedom in the molecules generally that may have large absorption coefficiency in infrared band such as CO_2.

Absorption coefficiency:

Large absorption coefficiency has small affect on flame spread in normal gravity, but it has great impact in microgravity. The re-absorption effect increases the temperature of the preheat zone that leads to very robust flame in microgravity especially in a quiescent condition.

These effects couple each other and can move the microgravity-regime limit. For example, at 30% O_2 level, the microgravity limit is about 10cm/s for N_2 balance. On the other hand, it is more than 16cm/s for He balance, and it is about 5cm/s for CO_2 and Ar balance conditions. As a result, CO_2 is an excellent extinguishant in normal gravity, but it is not always excellent in microgravity; the flame is robust in CO_2 balance. Therefore, when discussing the flame spread in microgravity, we have to pay attention how the flame deviates from the thermal-regime. The dimensionless loss number, R_{loss}, in Eq. 6 may be helpful to estimate the "critical flow velocity" below which the flame cannot spread.

Acknowledgements

This study is carried out as a part of Ground Research Announcement for Space Utilization promoted by Japan Space Forum, and also supported by Gifu-Prefecture Micro-Gravity Experiments Promoting Congress and NASA, Glenn Research Center through contract number NCC3-842.

Nomenclature

c_g	Specific heat of gas
c_s	Specific heat of solid
Da	Damkohler number
F	Flame constant, Eq. 2
L_g	Gas-phase diffusion length scale, m
L_{gx}	Gas-phase diffusion length scale in x-direction
L_{gy}	Gas-phase diffusion length scale in y-direction
L_{sx}	Length of the preheated solid phase
L_{sy}	Thickness of the preheated layer
R_{loss}	Total heat loss number, Eq. 6

R_{rad} Radiation number, Eq. 7
R_{side} Side loss number, Eq. 8
T_f Characteristic (adiabatic) flame temperature
T_v Constant vaporization temperature
T_∞ Ambient temperature
t_{res} Residence time in gas or solid phase
t_{chem} Chemical reaction time in gas phase
V_g Velocity of the oxidizer
V_f Absolute spread rate
V_r Velocity relative to the flame, Vr=Vg+Vf
W Width of the fuel in z-direction

Greek Symbols

α_g Thermal diffusivity of gas, evaluated at Tv
α_s Thermal diffusivity of solid
α_{abs} Absorption coefficiency of gas
ε Surface emissivity
λ_g Gas-phase conductivity evaluated at Tv
λ_s Solid-phase conductivity
η Non-dimensional spread rate, Eq. 5
ρ_g Gas density evaluated at Tv
ρ_s Solid density
τ Fuel half-thickness

References

1) Takahashi, S., Kondou, M., Wakai, K., and Bhattacharjee, S., *Proc. Combust Inst.* **29**, 2579-2586, 2002.
2) Bhattachrjee, S., West, J., and Altenkirch, R. A., *Proc. Combust. Inst.* **26**, 1477-1485, 1996.
3) Bhattacharjee, S., King, M. D., Takahashi, S., Nagumo, T., and Wakai, K., *Proc. Combust. Inst.* **28**, 2891-2897, 2000.
4) Takahashi, S., Nagumo, T., Wakai, K. and Bhattacharjee, S., *JSME International Journal, Series B*, **43**(4), 556-562, 2000.
5) Bhattacharjee, Wakai, K, and Takahashi, S., *Combust. Flame*, **137**, 506-522, 2004.
6) Bhattacharjee, Ayala, R., Wakai, K, and Takahashi,S.,*Combust. Inst.* **30**, 2279-2286, 2004.
7) T'ien, J.S., *Combust. Flame* **65**, 31, 1986.
8) Olson, S.L., Ferkul, P.V., T'ien, J.S., *Proc. Combust. Inst.* **22**, 1213–1222, 1988.
9) Bhattacharjee, S., Altenkirch, R.A., *Proc. Combust. Inst.* **23**, 1627–1633, 1990.
10) Reid, R. C., Pravsnitz, J. M., Sherwood, T. K., The properties of Gases and Liquids, McGraw-Hill, 1977.
11) Grosshandler, W. L., RADCAL: A Narrow-Band Model for Radiation Calculations in a Combustion Environment, NIST Tech. Note 1402, 1993.
12) Fernandez-Pello, A.C., Ray S.R., and Glassman, I., *Proc. Combust. Inst.* **18**, 579, 1981.
13) Chen, C.H., *Combust. Sci. Technol.* **69**, 63–83, 1990.
14) Son, Y. and Ronney, P. D., *Proc. Combust. Inst.* **29**, 2587-2594, 2002.

Received October 23, 2006
Accepted for publication, July 1, 2007